PAPER

Check for updates

Impact of size and UV-ageing of polystyrene nanoparticles on copper(II) adsorption: kinetics and isotherms in aquatic environments†

Shadab Soheilian, [iD][a] Beth Jordan,[a] Fiona L. Hatton, [iD] *[a]
Eugenie Hunsicker[b] and Zhaoxia Zhou [iD] *[a]

There has been substantial concern over the potential for microplastics to serve as vectors for toxic heavy metals through adsorption. The mechanisms involved in this process are particularly understudied in the context of nano-sized particles. To address this gap, we report the adsorption of Cu^{2+} ions to polystyrene nanoparticles (PS-NPs) in simulated aquatic environmental conditions, with and without UV-ageing. Surfactant-free PS-NPs were synthesised with average diameters of 130, 260 and 520 nm. Scanning electron microscopy and dynamic light scattering characterisation of PS-NPs revealed increased instability and aggregation with decreasing particle size, following UV-ageing. While PS-130 nm initially exhibited higher Cu^{2+} adsorption capacity in DI water, this value shifted in favour of PS-260 nm after UV-ageing, due to higher colloidal instability of PS-130 nm. Yet, in seawater, 3–4 times reduction in adsorption was observed for all the samples, compared to DI water, alongside accelerated equilibrium times, attributed to the competition of ions in seawater. On the surface of UV-aged PS-NPs, X-ray photoelectron spectroscopy analysis showed an increase in $Cu(OH)_2$ bonds after adsorption, resulting in increased activation energy of adsorption compared to original samples. Adsorption isotherms favoured the Freundlich model, highlighting a distinct isotherm shape for each medium and a tendency toward a linear isotherm as the particle size and/or temperature increased. This research enhances our understanding of PS-NPs behaviour in aquatic environments, paving the way for exploring metal ions' interaction with complex plastic nanoparticles in future studies.

Environmental significance

One of the challenges with micro- and nano-plastics is their ability to adsorb and transport toxic heavy metal ions over long distances in aquatic environments. While these particles are concerning, knowledge of this adsorption behaviour is limited, especially for nano-sized particles. This study investigates the adsorption of copper(II) ions by nano-sized polystyrene nanoparticles (PS-NPs) in aquatic environments. Investigating UV-ageing behaviour of PS-NPs and its influence on metal ion adsorption, alongside other environmental factors, reveals their interaction mechanisms in greater depth. These findings provide insights into nanoparticle behaviour and underscore potential hazards in aquatic environments. Emphasizing the need for further research to understand and mitigate their environmental impact, in terms of the interactions between metal ions and plastic nanoparticles.

1 Introduction

Microplastics are known to exhibit a strong affinity for adsorbing heavy metals through various mechanisms.[1–3] Their capacity to adsorb high amounts of these pollutants especially in aquatic environments, coupled with their persistence, enhance their ecological hazards, such as causing immunotoxicity and phytotoxicity in micro-organisms.[4] Polystyrene (PS) stands out as one of the most abundant microplastic particles in marine environments, and can be found in a broad size range (5 mm down to a few nm).[5–7] PS microplastics showed high affinity to different heavy metals, namely Cd,[8] Sr,[9] Pb,[2] Cu,[10] As[11] and Cr.[12]

Various studies have demonstrated the toxicity of metal-adsorbed PS microplastics to living organisms. For instance, oxidative damage and inflammation occurred in zebra fish tissue when exposed to combined Cd and PS microplastics.[13]

[a] *Department of Materials, Loughborough University, Loughborough, LE11 3TU, UK*

[b] *Department of Mathematical Sciences, Loughborough University, Loughborough, LE11 3TU, UK*

† Electronic supplementary information (ESI) available. See DOI: https://doi.org/10.1039/d4en00433g

548 | *Environ. Sci.: Nano*, 2025, **12**, 548–562

This journal is © The Royal Society of Chemistry 2025

The chemodynamics and bioavailability of metal ions can also vary based on the physicochemical features of the organisms and the aqueous environment. As an example, metal ions can be released at a higher rate in acidic conditions found in gut or lysosomal environments.[14] However, studies showed that nanoplastics (i.e., microplastics <1000 nm (ref. 15)) might be of more concern as carriers of heavy metals as they have an increased adsorption ability due to their larger surface area, making them more susceptible to weathering and further enhancing their adsorption capacity.[16,17] Despite the environmental significance of nanoplastics and the fact that nanoparticles are known to behave differently from their larger counterparts,[18] information on their interaction with heavy metals is limited.

There is evidence that PS nanoparticles (PS-NPs) with heavy metal contaminants can be digested by living organisms, affecting their metabolism.[19] Qiao et al. reported that PS nanoplastics (100 nm) adsorb more Cu than 20 μm PS microplastics, accelerating the accumulation of Cu in the livers of zebra fish in a size-dependent manner, leading to increased levels of specific antibodies.[20] This suggests that size of the particles can significantly influence ecotoxicological impacts of them. Despite the high affinity of PS-NPs for metal ions and their known ecological hazards to various living organisms, the interaction between these nanoparticles and heavy metals remains largely unexplored. This is particularly true regarding the effect of environmental weathering on the adsorption process.

Solar UV-induced photodegradation serves as the primary degradation pathway for PS-NPs in the environment, inducing surface modifications such as oxidation on polymer surfaces, which affects the uptake of contaminants.[21] Moreover, with smaller particle sizes, thus increased specific surface area (SSA), surface reactivity is elevated and surface alterations are enhanced due to interactions with the surrounding media.[22] Mao et al. showed a direct relationship between the degree of UV-ageing and the adsorption capacity of heavy metals by PS particles.[23] Higher surface area leads to an increased amount of polar functional groups such as aldehydes, ketones, and carboxylic acids after UV-ageing.[23,24] For PS particles, reactive oxygen species (ROS) created during UV-ageing, including $^{\bullet}OH$, $O_2^{\bullet-}$, and $^1O_2$, induce the formation of oxidative functional groups.[25] In the case of PS particles, excitation of the phenyl ring during UV-ageing may lead to chain scission or cross-linking and the creation of carbonyl groups.[26] The formation of these additional functional groups on the surface of PS particles during UV-ageing was shown to affect the interaction of heavy metals through surface oxidation.[8,27]

Additional functional groups resulting from UV-ageing can enhance adsorption capacity,[23,28,29] by forming metal complexes via mechanisms such as electrostatic interactions or hydrogen bonding.[4] This can, in turn, enhance their ecological hazards in the environment. For example, immobilization of the water flea, Daphnia magna, was higher when exposed to Ni and carboxylic acid functionalised polystyrene (PS) nanoparticles than when exposed to Ni and unmodified PS nanoparticles.[30] Recent research commonly suggests physical adsorption in form of electrostatic attraction as the predominant interaction between heavy metal ions and plastic particles.[31] Dong et al. highlighted electrostatic forces as a key mechanism in the adsorption of As(III) onto ball-milled PS fragments.[32] Beside particle size and weathering effects, environmental factors also affect the adsorption rate. For example, the ionic strength of the environment can reduce adsorption by decreasing the available sorption regions.[4] This integrated perspective underscores the importance of considering the interplay of multiple factors in understanding the complex fate of nanoplastic particles in aquatic environments.

Despite the wide range of PS particles in aquatic environments down to the nanometer scale, limited information exists on the adsorption mechanisms and size-dependent interactions of PS-NPs with heavy metals. Additionally, information regarding adsorption kinetics of PS-NPs and the impact of UV-ageing on this process remain largely unexplored. One challenge in this field lies in the limited availability of nanoplastics for environmental studies. Due to their small size, nanoplastics are challenging to detect and recover, and their size distributions have been found to vary across locations.[5] Moreover, their unknown exposures in the environment limit studying their degradation patterns and heavy metal adsorption in a controlled manner.

In studies where heavy metal adsorption to nanoplastics is targeted, typically, the techniques employed to generate plastic particles below 1 μm result in polydisperse particles with a broad particle size distribution. Top-down methods, such as mechanical techniques like ball milling and sieving,[33–35] as well as bottom-up methods like precipitation methods,[36–38] resulted in diverse size ranges, demonstrating the challenge with obtaining precise control over particle size using these methods. On the other hand, commercial reference nanoparticles, despite the narrow size dispersity, may not be well-suited for environmental research due to the potential presence of surfactants on their surface. Additionally, these particles might be prohibitively expensive to obtain in the quantities necessary for this research. In environmental studies, plastic particles should ideally retain their original chemical composition and demonstrate stability that closely mimics the natural colloidal properties of nanoplastic particles, while also minimizing the likelihood of surfactant contamination. Enabling access to these nanoparticles is essential for research, and achieving this goal relies on creation of the particles with controlled size dispersion using affordable and efficient methods. While these particles may not precisely replicate real environmental particles, they serve as reliable models to simulate their behaviour in a laboratory setting.

In this study, surfactant-free emulsion polymerization was employed to produce narrowly dispersed and stable polystyrene (PS) nanoparticles, allowing for precise size control. PS-NP sizes were selected based on the twofold increase in average diameter within the series (130, 260 and 520 nm). The subsequent exploration focused on UV ageing of the PS-NPs, monitoring variations in particle size, charge

This journal is © The Royal Society of Chemistry 2025

Environ. Sci.: Nano, 2025, 12, 548–562 | 549

and chemical composition exhibited by three distinct particle sizes. For heavy metal adsorption experiments we targeted copper as it is one of the most abundant metal pollution released to water resources, coming from multiple technological, domestic and industrial applications.[39] The kinetics and isotherms of Cu^{2+} adsorption were investigated for both original and UV-aged samples in two aqueous media —DI water and seawater—across a temperature range of 290–310 K. Calculation of activation energy provided a better understanding of the interactions between the metal ions and the surface of the particles.

2 Materials and methods

2.1 Materials

For the synthesis of PS-NPs, potassium per-sulfate (KPS) and styrene monomer both from Sigma-Aldrich Co. with purity of ≥99% and methanol (99%, Thermo Scientific Co.) were used. Deionized (DI) water with electrical resistivity of ≥18 MΩ were employed throughout the experiments. The Cu^{2+} adsorption experiments were demonstrated using the metal compound of $CuSO_4 \cdot 5H_2O$ (≥98%, Sigma Aldrich Co.). The artificial seawater consisted of $MgCl_2 \cdot 6H_2O$ (≥99%, Millipore Co.), NaCl, Na_2SO_4, $CaCl_2$, KCl, $NaHCO_3$, KBr, H_3BO_3, $SrCl_2$ and NaF all obtained from Sigma-Aldrich Co. with purity of ≥99%. The artificial seawater was prepared in the lab as detailed in Table S1,† and the molarity of each ion in seawater is shown in Table S2.†

2.2 Synthesis of PS-NPs

Surfactant-free emulsion polymerization in a methanol-enriched aqueous medium was used to synthesize narrowly dispersed PS-NPs.[40] A reactor was charged with DI water (100 g), methanol (50 g), and styrene monomer (2.5 g). The polymerization was conducted at 70 °C with a constant stirring rotation of 100 rpm. The mixture was degassed under a nitrogen atmosphere, stirred for 15 minutes, and then heated to 70 °C. The polymerization was initiated with a KPS solution (0.0125 g) dissolved in 10 mL of water, which had been degassed under nitrogen. The polymerization reaction proceeded for 24 hours before being cooled to room temperature and exposed to air to quench the reaction. Methanol in the solution was removed by rotary evaporation. A rotary evaporator (Buchi F401, Buchi Ltd, Switzerland) with a water bath (Buchi 461, Buchi Ltd, Switzerland) at a temperature of 40 °C was used for 30–45 min. Removal of methanol was confirmed by ^1H nuclear magnetic resonance (NMR) spectroscopy analysis of the dispersions, data not shown. Polymerisation conversion rates were determined gravimetrically using a moisture analyser (Ohaus MB23, Ohaus Corp., UK). 3 mL of the synthesized suspension was added to the analyser pan. The moisture analyzer was set to measure the percentage of remaining solid content in the sample as it was heated at 120 °C. The conversion rate (eqn (S1)†) was obtained using theoretical solid content at 100% monomer conversion (eqn (S2)†). Distribution of the particle size determined by dynamic light scattering (DLS) analysis.

The choice of specific order of particle sizes in this study allowed for a systematic approach to observe size-dependent changes on the nanoscale, providing comprehensive insights into the environmental impact of PS-NPs across different size ranges in aquatic environments. Therefore, for this study, we selected three distinct particle diameters—130 nm, 260 nm, and 520 nm—showing narrow dispersity with a high conversion rate of approximately 95%.

2.3 UV-degradation process

Synthesized PS-NPs, at a concentration of 0.05%wt, were exposed to a 36 W UVA lamp with a wavelength of 360 nm. The irradiance was measured directly at the sample's position in the lab using a UV-A radiometer showing a value of 127 W m^{-2}. Quartz cuvettes were used as sample containers to prevent interference of the UV light with the container walls. The samples were exposed to UV light for different time intervals up to 12 days. To ensure the accuracy and reliability of the UV ageing changes, control samples with the same concentration were kept in a dark place as part of the experiment.

2.4 Adsorption process of Cu^{2+} ions

To study adsorption kinetics, original and UV-aged PS-NPs with concentration of 0.1 g L^{-1} were mixed with a 10 mg L^{-1} Cu^{2+} solution using $CuSO_4 \cdot 5H_2O$. This concentration was chosen based on previous studies[32] and environmental concentrations of copper.[41] Two different solvents, DI water and simulated seawater, were utilized. A 20 ml mixture was stirred at a temperature of 290 K, with a speed of 100 rpm, and sampling was conducted at various time intervals up to 10 hours. To ensure that PS particles were solely responsible for adsorbing metal ions, a control sample was included to address any other factors affecting the adsorption process. In this experiment, the control sample was Cu^{2+} solution with precisely the same concentration without PS particles. In order to determine the activation energy of the adsorption process, the adsorption kinetics were repeated at temperatures of 300 K and 310 K.

To investigate the adsorption isotherm, a range of Cu^{2+} solutions, spanning concentrations from 10 to 50 mg L^{-1} in both DI water and seawater were mixed with PS-NPs at a concentration of 0.1 g L^{-1} at temperatures of 290 K, 300 K or 310 K to achieve equilibrium adsorption. Sampling occurred at the initiation of PS-NPs introduction and upon reaching equilibrium. The process of adsorption kinetics and isotherms was repeated three times for each setting.

2.4.1 Fitting adsorption kinetic models. For studying adsorption kinetics, pseudo-first-order (PFO) and pseudo-second-order (PSO) are two commonly used kinetic models that describe the adsorption rate of adsorbates onto the surface of adsorbents.[42] Pseudo-first order (PFO) kinetic models is described as below:

$$q_t = q_e(1 - \exp(-k_1 t)) \qquad (1)$$

where q_t and q_e are the amount of solute adsorbed at time t and at equilibrium, respectively. The value of k_1 is the rate constant of the PFO model. The pseudo-second-order (PSO) model can be expressed as:

$$q_t = q_e \left(\frac{k_2 q_e t}{1 + k_2 q_e t} \right) \tag{2}$$

where k_2 is the rate constant of the PSO kinetic model.

While R-squared, R^2, is a valuable criterion for identifying a model that matches experimental data, it is not independently sufficient. Therefore, in addition to R^2, theoretical value of q_e, denoted as $q_{e,Cal}$, obtained during the fitting process in Python, was used for both models to determine which one closely anticipates the experimental value.

2.4.2 Calculation of activation energy. After finding the best fitting for adsorption kinetics data at different temperatures, the related k value was applied in Arrhenius equation as below:

$$\ln k = \ln A - \frac{E_a}{RT} \tag{3}$$

where A is Arrhenius factor, R is the universal gas constant (8.31 J per mole per K), T is the temperature (K) and E_a is the activation energy (J mol^{-1}). By having equilibrium adsorption constant, k values, across different temperatures, E_a can be determined.

2.4.3 Fitting adsorption isotherm models. Langmuir and Freundlich adsorption models are the most famous models that can reliably predict the adsorption isotherm by polymeric particles.[43] Langmuir isotherm model is based on the assumption that active sites are homogeneously distributed on the surface of the adsorbents which are limited in number and energetically independent from each other with no lateral interaction.[44] In this model, a maximum adsorption capacity (q_m) is considered when the adsorbent's surface is covered with a monolayer.[45,46]

$$q_e = \frac{q_m K_l C_e}{1 + K_l C_e} \tag{4}$$

where K_l is the Langmuir constant and C_e (mg L^{-1}) is the adsorbate concentration in the liquid phase.

Unlike the Langmuir model, the Freundlich isotherm model represents non-linear multilayer adsorption.[47] This model has been derived from the assumption that the adsorption sites are distributed heterogeneously.

$$q_e = K_f C_e^{1/n} \tag{5}$$

where K_f is Freundlich constant and, $1/n$ is the heterogeneity factor, showing the distribution of adsorption sites on the surface of particles.[48] A value $1/n < 1$ suggests uneven adsorption sites, while $1/n = 1$ reduces it to a linear model. Linear forms of eqn (4) and (5) were employed for data fitting processes, as shown in eqn (S3) and (S4).†

2.5 Characterisation methods

Z-Average diameters and size distribution of the particles was examined by DLS (Zetasizer Ultra, Malvern Pananalytical

Corp., UK) at temperature of 25 °C, and the equilibration time of 120 s. The measurements were repeated 3 times for each sample. The electrophoretic mobility of the samples was determined using the same instrument employing a folded capillary zeta cell (Malvern PANalytical DTS1070). The morphology of the particles was studied using field emission gun scanning electron microscope (FEGSEM, JEOL 7100 A, JEOL Ltd, Tokyo Japan) at the voltage of 5 kV. 40 μL of the PS solution in water with concentration of 0.05%wt was deposited onto a copper tape and dried under ambient conditions overnight before being coated with gold and palladium (Au/Pd) with the ratio 80/20 using a rotary pumped coater (Q150R S Plus, Quorum Corp., UK) for 90 s. To confirm chemical structure of the particles, FTIR (Nico-letTM iN10 MX Infrared Imaging Microscope) in transmission mode was utilized using a CaF$_2$ window in the wavelength range of 400–4000 nm and collection time was 25 s resulting in 256 scans taken. The concentration of Cu^{2+} ions in the liquid phase before and after adsorption was analysed by UV-vis spectroscopy (Cary 5000 UV-vis–NIR, Shimadzu Corp., UK) using quartz UV-vis cuvette with wavelength range of 200–1200 nm. Prior to the analysis, samples were centrifuged using a mini centrifuge (Eppendorf MiniSpin® Plus, India) at 12 000 rpm for 30 minutes with RCF of 10 800g to remove PS-NPs that had incorporated adsorbed Cu^{2+} ions. Fig. S1† shows the UV-vis spectra of the samples before and after centrifugation, indicating that no PS or other species remained in the supernatant after removal that could interfere with the Cu^{2+} UV-vis peak at 800 nm. For quantitative analysis, a calibration curve was established using known concentrations of Cu^{2+} ions, as shown in Fig. S2.† The adsorbed mass of Cu^{2+} ions at time t, q_t (mg g^{-1}), were calculated using eqn (S5).† Surface chemical modifications post UV-ageing and Cu^{2+} bonding on the surface of PS-NPs were analysed using X-ray photoelectron spectrometer (XPS) (Thermo Scientific K-Alpha, UK). PS solution with a concentration of 0.05%wt was deposited onto a silicon wafer. Prior to deposition, the silicon wafer underwent cleaning using a UV/ozone sample cleaner (ZONESEM, Hitachi High-Tech, Canada Inc.) for 15 minutes. The samples were dried under ambient atmosphere overnight. The charge is referenced to the adventitious C 1s with the C–C peak at 284.8 eV.

3 Results and discussion

In this study, we conducted a thorough investigation into the physical and chemical properties of the PS-NPs particles, before and after UV-ageing, focusing on size-dependent changes. On the adsorption between PS-NPs and Cu^{2+} ions, we examined how the adsorption mechanism is influenced by UV-ageing. Our research also included studying the adsorption kinetics and isotherms of PS-NPs, considering influential factors of particle size, UV-ageing, medium and temperature. These findings contribute to our understanding of the potential hazards posed by PS-NPs in aquatic environments when exposed to heavy metal ions.

3.1 Analysis of synthesized PS-NPs

PS-NPs were synthesised by surfactant free emulsion polymerisation in the presence of methanol. Surfactant-free emulsion polymerisation is a convenient method to prepare PS particles without the need for surfactants or other additives,[49] which are commonly found in commercially sourced PS particles.[50] To synthesize particles of distinct sizes, various methanol-to-water ratios were employed, as well as different ratios of styrene and KPS, as illustrated in Table S3.† An increase in the water-to-medium ratio, along with a decrease in the ratio of styrene-to-medium and KPS-to-styrene, resulted in the reduction of PS particle size. Through systematic screening of polymerisation conditions, the resultant nanoparticle size could be tuned between 120–760 nm. Here, we targeted three PS-NPs with varying diameters, denoted as PS-130, PS-260, and PS-520, with average diameters of 130 nm, 260 nm, and 520 nm, respectively, as highlighted in Table S3.† Polydispersity index (PDI) values for these samples were less than 0.05 and PDI values for other synthesised particles can be found in Table S3.† The FTIR analysis conducted on the synthesized PS-NPs, as illustrated in Fig. S3,† revealed a 96.80% similarity with atactic or general-purpose polystyrene as per the Hummel Polymer library for all three samples.
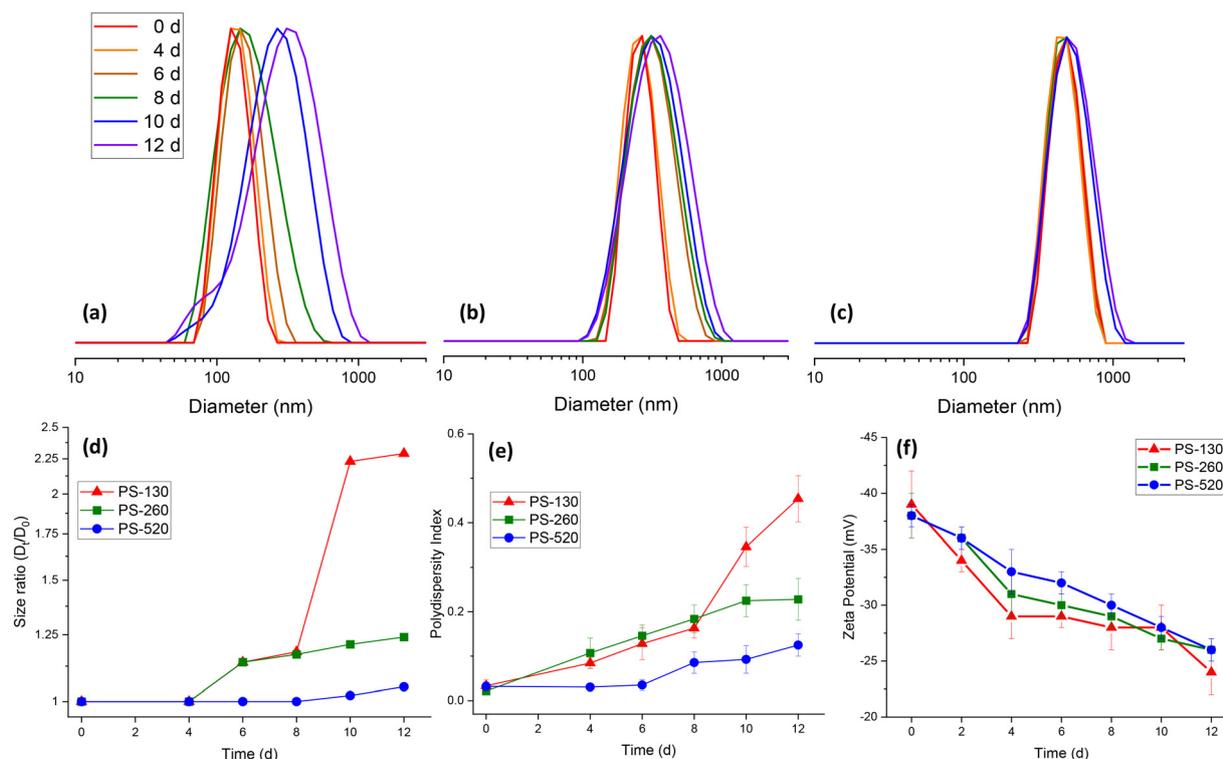
3.2 UV-degradation analysis

To evaluate the influence of exposure to UV radiation on the particles, size distribution of PS-NPs during UV-ageing were studied using DLS (Fig. 1(a–c)). For each sample, the Z-average diameter increased with UV exposure, see Fig. 1(d). However, this increase was more prominent for the smaller particles, PS-130, which increased from 130 nm to 297 nm after 12 days of exposure. Whereas, PS-260 increased from 260 nm to 322 nm, and PS-520 only increased up to 546 nm after 12 days UV exposure. Moreover, the polydispersity index (PDI), in Fig. 1(e) increased with UV-exposure time. This was also more prominent for the smaller particles, PS-130, increasing from 0.032 to 0.454, while the PS-260 and PS-520 increased to 0.228 and 0.125, respectively.

Studying morphological changes using scanning electron microscopy (SEM) proved much higher tendency for the smaller particles, PS-130, to aggregate as well as a partial morphological change from their original spherical shapes for some of the particles (Fig. 2(a and b)). Larger particles, due to less SSA and less surface reactivity, remain their original morphology (Fig. 2(c–f)) and deformation primarily manifested as small surface flakes and surface layering which can be the reason of slight increase in Z-average diameter in DLS analysis of these samples.

The electrophoretic mobility of the particles was assessed by measuring the zeta potential (ZP) during UV exposure. In all cases, the synthesised particles were negatively charged with ZP between −37 to −39 mV. This anionic character is imparted by the persulfate initiator used in the surfactant-free emulsion polymerisation procedure, resulting in anionic sulfate groups ($-SO_4^-$) at the PS-NP surface.[49] However, for all

Fig. 1 (a–c) Size distribution by intensity of DLS analysis, (d) size changes of the particles relative to initial size*, (e) polydispersity index of DLS analysis and (f) zeta potential of the particles at different time intervals during UV-degradation. Error bars represent the standard deviations. *D_0 and D_t represent initial diameter and the diameter at time t, respectively.
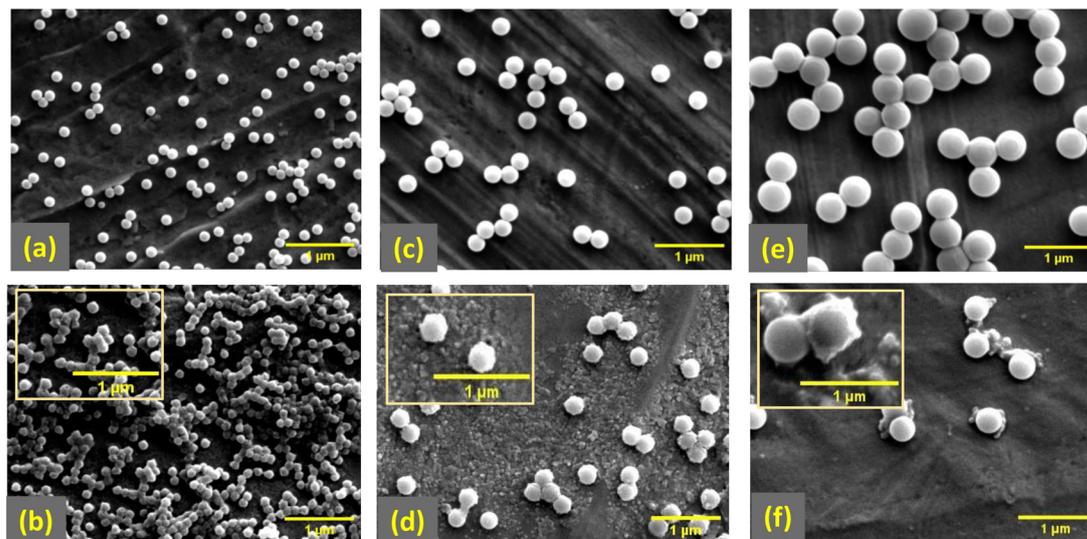
Fig. 2 SEM images of (a and b) PS-130, (c and d) PS-260 and (e and f) PS-520 in their original and UV-aged forms, respectively.

the PS particles, upon UV exposure the observed ZP became less negative, tending towards approximately −25 mV (Fig. 1(f)). This reduction in anionic character is likely due to loss of the sulfate groups, which can be cleaved during UV-aging. Loss of surface charge would also explain the increase in particle size and PDI due to particle destabilisation and aggregation (Fig. 1). This has previously been reported during

aggregation studies of PS-NPs exposed to UV irradiation with differing surface functionalities.[50]

As discussed earlier, the patterns of morphological and size changes vary among PS-NPs within the size range of 130–520 nm. To comprehend the underlying reasons for these variations, it is essential to investigate surface chemical modifications on the particles' surfaces as a result of UV-
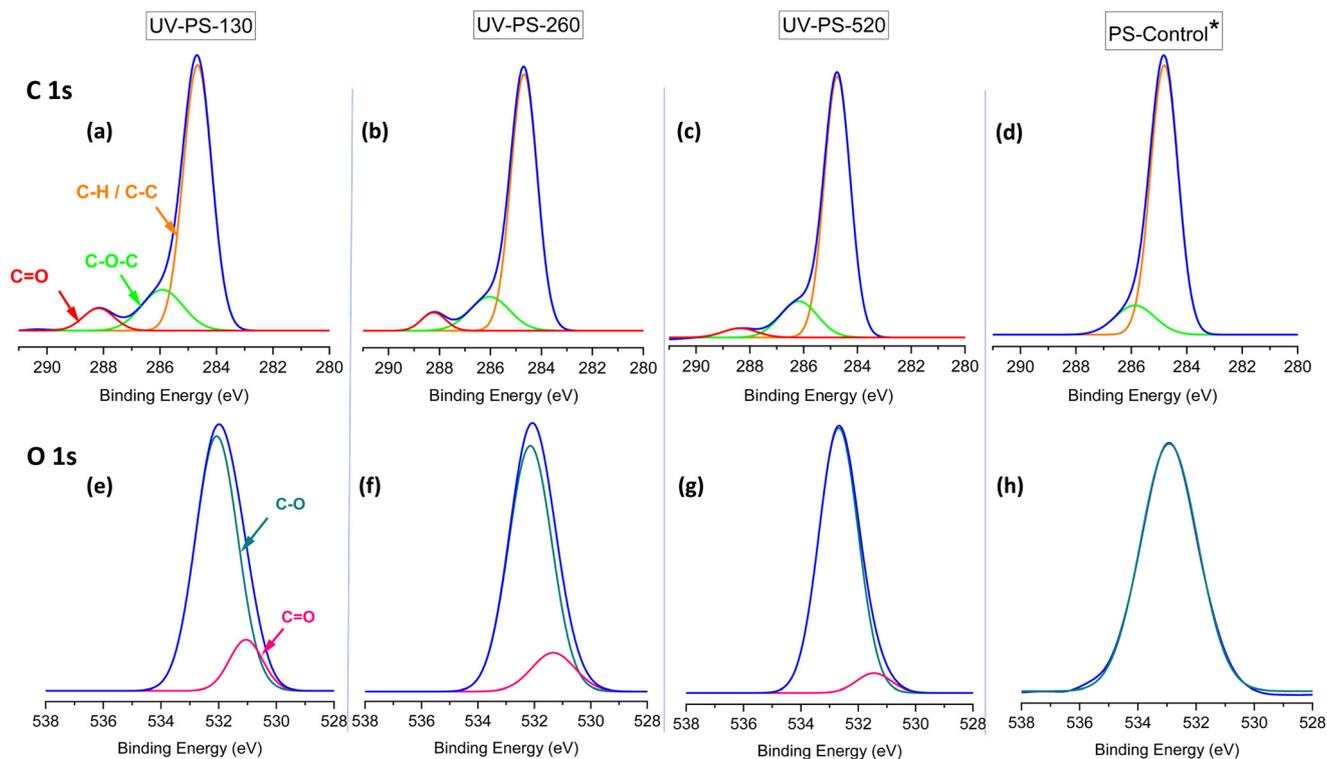

Fig. 3 (a–c) C 1s and (e–g) O 1s XPS spectra of UV aged PS particles compared to (d and h) the corresponding spectra of the control samples. To prevent redundancy, only the peak corresponding to one of them is depicted here. *The XPS spectra associated with control samples across all size ranges exhibit a uniform shape (refer to Fig. S4†).

degradation. The XPS spectra of C 1s and O 1s provide information about surface modifications of PS particles and distinct bonds associated with specific binding energies related to each element (Fig. 3). Although there is no oxygen in the structure of PS particles, the O 1s peak associated with oxygen is observable in XPS analysis, since the samples contain oxygen, stemming from factors such as the persulfate initiator used in synthesis, adventitious contamination, oxidation, or moisture.[51] However, this peak was useful to compare the amount of oxygen bound to the surface *via* different carbon bondings across the samples before and after UV-ageing.

In UV-aged samples, C 1s and O 1s XPS spectra underwent surface changes influenced by the ageing process. C 1s XPS analysis in Fig. 3(d), alongside the primary C–C peak at 284.8 eV, revealed the presence of a C–O peak at 286 eV for the original samples, potentially formed during synthesis or sample preparation and their interaction with water molecules.[32] In UV-aged samples in Fig. 3(a–c), an additional peak corresponding to C=O emerged at a binding energy of 288.5 eV due to the UV-degradation process. The intensity of this C=O peak increased with a concomitant reduction in particle size and increased ZP (*i.e.*, became less negative). The changes in O 1s XPS spectra following UV-degradation approved the creation of C=O peak, which can be seen in Fig. 3(e–g), compared to the O 1s spectra of control samples in Fig. 3(h). This increase in carbonyl functionality could be due to the formation of new aldehyde, ketone or carboxylic acid groups, which are known to form during UV aging of PS.[25,26] Whilst carboxylate groups would introduce anionic character, as we observed an increase in ZP for all PS-NPs (from approx. −40 to −25 mV), our data indicates that the PS-NPs became less anionic. This is most likely due to photodegradation of sulfate groups[50] and we infer that the increase in C=O content may be predominantly ketone or aldehyde, rather than carboxylate groups. The loss of sulfate functionalities could not be explored by XPS as demonstrated in previous work,[50] as the amount of sulfur present was below the detection limit of the equipment.

To quantitatively assess the ratio of each element and related functional groups, it is necessary to consider the area under the related peaks. The ratio of peak areas related to O 1s and C 1s yields the O/C ratio (Table 1), which is indicative of the oxidation level on the particle's surface. As shown in Table 1, the initial O/C ratio varied within the range of 0.20–0.26 across different samples with standard deviation of ±0.13. However, after UV-ageing, O/C ratio increased up to approximately 2.7–4,

showing that PS-130 exhibited a 20-fold increase in the O/C ratio after UV ageing, while PS-260 and PS-520 showed approximately 13 to 14-fold increases. The standard deviation also increased up to 0.21 after UV-ageing, possibly due to uneven oxidation in different parts of the sample. Despite this, the deviation in the O/C ratio were smaller than the overall changes, indicating sufficient accuracy for comparison.

In quantifying the peaks associated with each functional group related to the C 1s XPS spectra (Table 1), the standard deviations were as low as nearly 1%. This consistency is because the shape of the C 1s spectra remained similar across different XPS measurements of a sample, ensuring that the corresponding ratio of each functional group remained almost constant, supporting the reliability of the data. For C–O groups, the increase was no more than 3–4% after UV ageing across different samples. An increase in the presence of C=O groups was also evident with decreasing particle size, rising from 3.49 to 6.57%, whereas this peak was not observed in control samples (Fig. 4).

3.3 Adsorption kinetics

Adsorption kinetics of Cu^{2+} ions by the original and UV-aged PS-NPs in DI water and seawater were analysed as shown in Fig. 4. Pseudo-first order (PFO) and Pseudo-second order (PSO) fittings were conducted on experimental adsorption kinetics based on eqn (1) and (2). The fitting parameters in Table 2 indicates that PSO yielded a better fit compared to PFO in terms of R^2 values. Also, the value of theoretical equilibrium adsorption of PSO, $q_{e2,Cal}$, for all samples are closer to experimental values, $q_{e,exp}$.

As shown in Fig. 4(a), it can be seen that in DI water smaller particles reached equilibrium faster, in 2 hours, while it took 4 hours for larger particles. According to recent studies on micro-sized particles and current results on nano-sized samples, shorter equilibrium times were observed by decreasing the size of particles. The enhanced diffusion characteristics exhibited by smaller particles, called diffusion-controlled mechanism, led to shorter equilibrium time. Consequently, this enhanced the transfer rate of metal ions to the surface of the adsorbent. A study conducted by A. A. Taha *et al.* proved the impact of this mechanism on the adsorption of heavy metals.[45] In Fig. 4(a), it can be seen that the adsorption for PS-130 is 6.20 mg g^{-1}, around 6 times more than PS-520, 1.05 mg g^{-1}. However, equilibrium times for PS-260 and PS-520 were almost identical. In this condition, the rate constants (k_2) also showed a decrease,

Table 1 The ratio of O/C related to C 1s and O 1s XPS spectra and percentage of functional groups in C 1s spectra for the PS-NPs before and after UV-ageing

Sample	Control particles			UV-aged particles		
	O/C	C–O (%)[a]	C=O (%)	O/C	C–O (%)	C=O (%)
PS-130	0.21 ± 0.11	13.23 ± 0.73	n.a.	4.27 ± 0.21	17.10 ± 1.05	6.57 ± 0.16
PS-260	0.26 ± 0.07	14.32 ± 0.86	n.a.	3.68 ± 0.13	15.54 ± 0.72	4.72 ± 0.08
PS-520	0.20 ± 0.13	13.33 ± 1.02	n.a.	2.72 ± 0.19	16.08 ± 0.91	3.49 ± 0.12

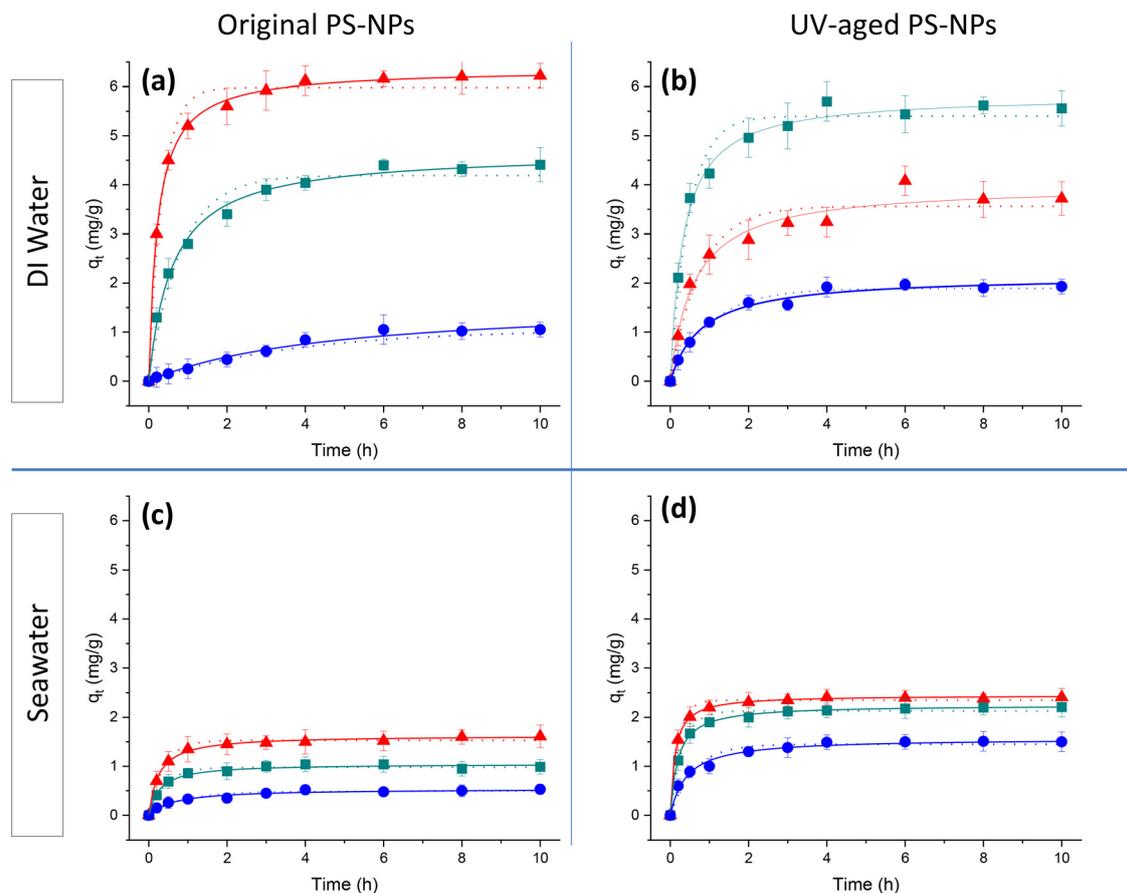[a] The peak area of each functional group was calculated as a percentage of the total C 1s peak.

554 | *Environ. Sci.: Nano*, 2025, **12**, 548–562

This journal is © The Royal Society of Chemistry 2025

Fig. 4 Adsorption kinetics of Cu^{2+} in (a and b) DI water and (c and d) seawater for original and UV-aged PS-130 (▲), PS-260 (■) and PS-520 (●), including PFO (dotted line) and PSO (solid line) model fittings.

Table 2 Fitting parameters of adsorption kinetics of Cu^{2+} ions by original and UV-aged PS-NPs in DI water and seawater

	Medium	Size (nm)	$q_{e,exp}$	PFO			PSO		
				$q_{e1,Cal}$	k_1	R_1^2	$q_{e2,Cal}$	k_2	R_2^2
Original PS	DI water	130	6.20	5.98	2.947	0.982	6.36	0.717	0.999
		260	4.41	4.19	1.233	0.971	4.67	0.357	0.995
		520	1.05	1.17	0.273	0.985	1.63	0.133	0.979
	Seawater	130	1.54	1.53	2.674	0.986	1.63	2.474	0.996
		260	1.02	0.98	2.401	0.984	1.05	3.458	0.986
		520	0.50	0.49	1.156	0.941	0.54	2.312	0.972
UV-aged PS	DI water	130	3.83	3.56	1.302	0.952	3.99	0.418	0.977
		260	5.58	5.40	2.097	0.978	5.83	0.522	0.994
		520	1.93	1.89	0.974	0.984	2.15	0.279	0.991
	Seawater	130	2.42	2.35	4.800	0.989	2.45	3.542	0.999
		260	2.19	2.13	3.300	0.989	2.25	2.347	0.999
		520	1.49	1.45	1.673	0.960	1.57	1.560	0.989

by approximately 2–2.5 times, with increasing particle size, indicating a higher rate of adsorption by smaller particles. Different studies have shown correlation between equilibrium adsorption and particle size, with smaller particles demonstrating higher adsorption capacities.[29,32]

By comparing adsorption kinetics of original and UV-aged samples in Fig. 4(a and b), a decrease in adsorption is observed for UV-aged PS-130. This occurred despite the increase of

carbonyl groups on the particle surface based on Fig. 3 and Table 1. And an increase in the equilibrium time (3–4 hours) was observed, primarily due to aggregation. This finding contrasts with recent studies on particles of micron or bulk dimensions, where adsorption increased by an order of 10 to 100-fold after UV ageing.[3,27] The observed variance could be attributed to the aggregation of nanoparticles in water following UV ageing, as opposed to their larger counterparts. The colloidal

This journal is © The Royal Society of Chemistry 2025

Environ. Sci.: Nano, 2025, **12**, 548–562 | **555**

instability following photodegradation of sulfate groups on PS-130 during UV-ageing led to higher polydispersity, aggregation and less available surface area for adsorption (Fig. 1).

In contrast to PS-130, PS-260 exhibited an increase in adsorption following UV ageing (Fig. 4(b)). This could be due to a reduced tendency of larger particles to aggregate after UV-ageing on one hand and creation of the oxidative functional group on the other hand. Hence, achieving a higher adsorption capacity necessitates finding the optimal degree of surface modification for the particles. This requires creating additional active sites on their surfaces while simultaneously ensuring a degree of stability in water to prevent excessive agglomeration.

By comparing adsorption kinetics in seawater in Fig. 4(c and d), it became evident that adsorption capacity in seawater was less than DI water by 3–4 times. This can be attributed to the decreased availability of active sites. Compared with DI water, seawater contains other salt cations (Ca^{2+}, Mg^{2+}, K^+, Na^+ etc., see Table S2†) in addition to the Cu^{2+}, which can compete to bind to the anionic PS-NPs.[17] This finding aligns with previous studies by Yu et al. demonstrating a decrease in the adsorption capacity of environmental metals with an increase in the salt content.[16] The reason behind this phenomenon lies in the competition between salt ions and metal ions for occupying the adsorption sites, where the presence of a high concentration of salt ions hinder the effective binding of metal ions to the active sites.[52]

Among the ions in seawater, divalent cations like Mg^{2+} and Ca^{2+} promote the aggregation of the PS particles in seawater due to forming cation bridging between negatively charged PS particles.[53] Therefore, they can strongly compete with Cu^{2+} for adsorption sites via aggregation and reduction of ZP, potentially reducing Cu^{2+} adsorption. Monovalent ions contribute to charge screening and ionic strength, influencing the electrostatic interactions and aggregation behavior of PS particles. Among monovalent ions, anions like Br^- and Cl^- affect the ionic strength and electrostatic environment and maintain the ionic balance of the suspension, while cations like Na^+ and K^+ neutralise the negative charge on the surface of PS-NPs. Therefore, they can also compete for adsorption sites, but their effect is less pronounced compared to divalent cations.[54]

The majority of the adsorption, in seawater, happened in the first hour of adsorption and equilibrium was reached faster due to fast occupation of salt ions on the surface of the particles. Furthermore, it is evident that the rate constant (k_2) decreased with increasing particle size. Moreover, the adsorption in seawater exhibits higher k_2 values compared to DI water, indicating differences in the number of active sites for each scenario.

In contrast to DI water, where particle agglomeration primarily stems from UV degradation processes, the presence of salt ions is main responsible for agglomeration in seawater. This lead to a notable increase in average particle diameters as depicted in Fig. 5. Consequently, the impact of agglomeration resulting from UV ageing can be considered negligible when evaluating the effects of seawater-induced
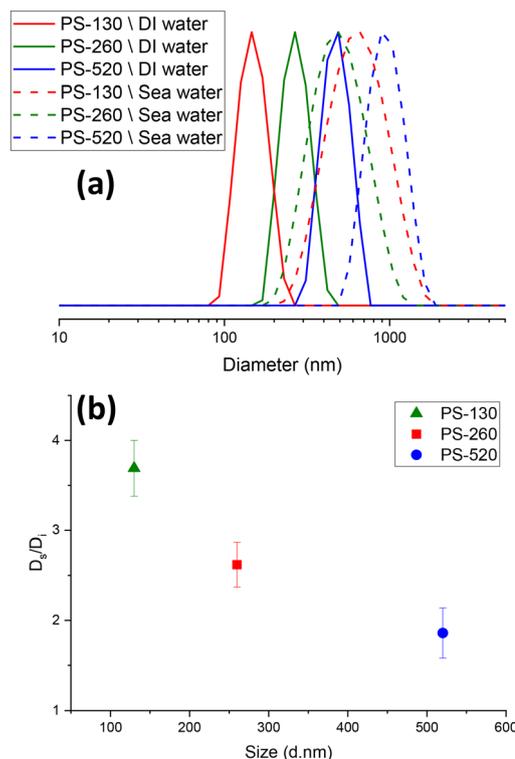

Fig. 5 Comparing (a) size distribution by intensity of DLS analysis for PS particles in DI water versus seawater and (b) particle size ratio of them (D_s and D_i are the particle size respectively in sea water and DI water.)

agglomeration. As indicated in DLS analysis of the samples in Fig. 5(a), particle size increased notably in seawater due to a reduction in surface electrostatic charge. Other studies have also demonstrated the rapid aggregation of nano-polystyrene in seawater.[55,56] Smaller particles, PS-130, exhibited a higher extent of agglomeration in seawater by 4 times (Fig. 5(b)). For PS-260 and PS-520, the corresponding value increases were 2.6 and 1.8 times, respectively. Hence, the adsorption rate in seawater was significantly reduced, compared to DI water. For UV-aged samples, although the particle size of UV-aged PS-130 in seawater was found to be slightly higher based on DLS analysis, the DLS peaks exhibited variability, likely stemming from the interaction between salt ions and PS-NPs. Considering this variability and the significant overlap in size distribution between PS-130 and PS-260 in seawater (Fig. 5(a)), the determining factor for adsorption lay in the surface properties of the particles. This underscores why the adsorption of PS-130 remained slightly higher than that of PS-260 in seawater, in both before and after UV-ageing.

To investigate the extent to which the adsorption was solely due to the surface area of the PS-NPs, the kinetics for the mass adsorbed based on the particles' specific surface area (SSA), $q_{t,SSA}$ (mg m^{-2}), was evaluated using the Z-average value of the particles for each condition (see Fig. S5 and Table S4†). Before UV-aging, PS-260 exhibited greater $q_{e,SSA}$ compared to PS-130 in DI water, possibly due to the colloidal nature of PS-130. Smaller particles, like PS-130, possess

higher surface energy and reactivity, resulting in increased energetic heterogeneity of active sites, thereby impeding homogeneous adsorption. This increased heterogeneity was further proven by isotherm studies, see section 3.5. However, as particle size further increased to PS-520, the SSA decreased significantly by fourfold compared to PS-130, reducing the number of active sites and diminishing $q_{e,SSA}$. After UV-aging, the $q_{e,SSA}$ difference between PS-130 and PS-260 increased, with severe aggregation of UV-aged PS-130 further impeding adsorption (Fig. S5(b)†). In seawater, the adsorption kinetics, based on the specific surface area (SSA) of the particles, showed that smaller particles exhibited higher adsorption both before and after UV ageing (Fig. S5(c and d)†), with the order of adsorption correlating with the SSA.

In terms of adsorption mechanisms between Cu^{2+} ions and surface of PS-NPs, the measurements in DI water showed ZP drop by half after Cu^{2+} adsorption from approximately −40 mV to between −20 and −25 mV for all the particles. This value in seawater showed a decrease from a range of −15 to −20 mV to between −5 to −8 mV (Table S5†). This screening of charges indicated the formation of electrostatic bonding between Cu^{2+} ions and surface of PS-NPs, where Cu^{2+} partially neutralised the negative surface charge of the PS-NPs. On the other hand, the UV-ageing process affected the adsorption mechanism of the Cu^{2+} ions by PS particles based on XPS analysis of Cu $2p_{3/2}$ peak in Fig. 6. The XPS analysis for these samples was conducted after thorough particle washing, effectively removing unbound Cu^{2+} ions from the surface of the particles after adsorption process. Compared to the XPS analysis of the original samples shown in Fig. 6(a–c), for UV-aged samples (Fig. 6(d–f)), alongside the peak related to copper(II) oxide (CuO) at 533.5 eV, an increase was observed in the peak associated with the bonding of $Cu(OH)_2$ at 534.7 eV.[57,58] The appearance of this peak is related to the surface modification as a result of UV degradation. Liu *et al.* also showed the different adsorption mechanisms for PS microplastics after UV ageing.[59] The adsorption between Cu^{2+} and PS particles involved metal–oxygen coordination bonding, in which the Cu^{2+} formed bonds with oxygen atoms from the functional groups of C=O and C–O (as shown in Fig. 3) present on the surface of the particles. In Fig. 6, the smaller peak of $Cu(OH)_2$ for larger particles indicates a reduced presence of oxygen-containing functional groups on the particle surface available for adsorption, which are aligned with the result of C 1s XPS spectra of UV-aged samples in Fig. 3.

3.4 Activation energy

Investigation of the activation energy (E_a) of the adsorption provides insights into the fundamental nature of the interaction. To achieve this, the adsorption kinetics experiment conducted at 290 K was repeated at temperatures of 300 K and 310 K, as illustrated in Fig. S6† and the corresponding k_2 values were determined (Table S6†). Subsequently, the activation energy was calculated using the Arrhenius equation (eqn (3)). Fig. S7† shows the Arrhenius plots of the Cu^{2+} adsorption in different conditions, where the slop of the fitted line represents the E_a value. The E_a and corresponding R^2 related to each fitted line are shown in Table S7.† Fig. 7 compares the activation energy, E_a in kJ mol^{-1}, of Cu^{2+} ions for both original and UV-aged samples.

The E_a values suggested the occurrence of physical adsorption for Cu^{2+} ions. Low E_a values, below 40 kJ mol^{-1}, indicate physical

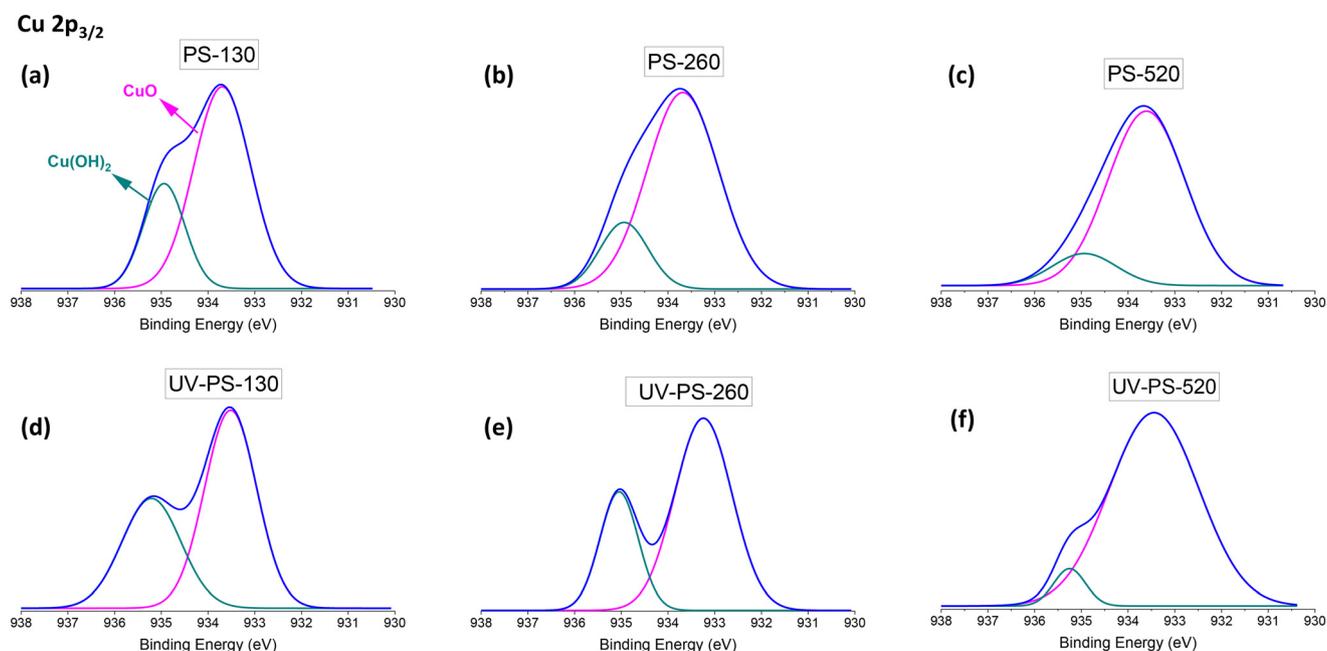**Fig. 6** Cu $2p_{3/2}$ XPS spectra of (a–c) original and (d–f) UV-aged PS-NPs after Cu^{2+} adsorption.

This journal is © The Royal Society of Chemistry 2025
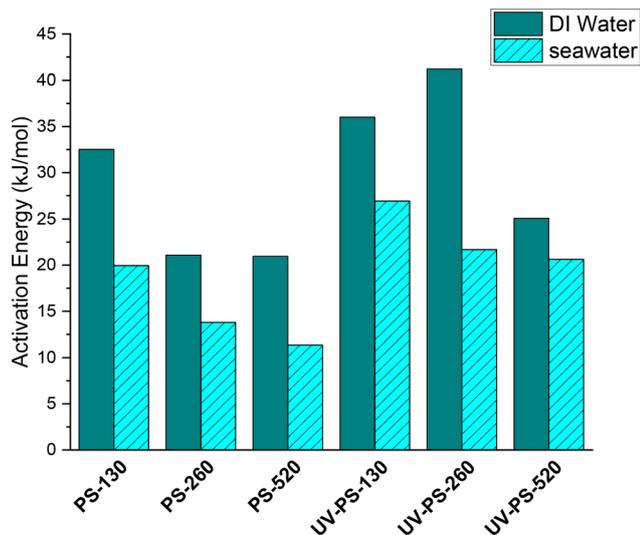
Environ. Sci.: Nano, 2025, **12**, 548–562 | **557**

Fig. 7 Activation energy (E_a) of Cu^{2+} adsorption by original and UV-aged PS particles in DI water and seawater.

sorption, while E_a in the range of 40–800 kJ mol^{-1} is associated with chemical sorption.[45,60] These findings align with previous studies on the E_a values for the adsorption of metal ions by plastic particles.[31,61]

The E_a values related to DI water (20–40 kJ mol^{-1}), as indicated in Fig. 7, were higher than those for seawater (10–28 kJ mol^{-1}). This difference can be attributed to the high ionic strength of seawater and the resulting charge screening effects on the surface of PS-NPs. On the other hand, the E_a values associated with UV-aged samples surpassed those of the original samples. This can be explained by the UV-induced surface modifications and the creation of C=O on the surface of UV-aged particles (Fig. 3), followed by an increase in $Cu(OH)_2$ based on the Cu $2p_{3/2}$ XPS analysis in Fig. 6. The increase in the bonding between Cu and OH in $Cu(OH)_2$, by higher binding energy, resulted in an increased activation energy for Cu^{2+} adsorption in UV-aged samples, due to the presence of metal-oxygen coordination bonds.

3.5 Adsorption isotherms

Fig. 8 shows the adsorption isotherm of Cu^{2+} by original and UV-aged PS-NPs in DI water and seawater at three different temperatures. Langmuir and Freundlich models were utilized to study the adoption isotherms of PS-NPs (see Section 2.4.3). Table 3 shows the relative coefficients of each isotherm model. It is evident that the Freundlich model provided a better fit, as indicated by the higher R^2 values obtained from this model. This model revealed the multilayer essence of adsorption on the surface of PS-NPs, in contrast to the homogeneous adsorption suggested by the Langmuir model. Higher Freundlich constants (K_f) for smaller particles are represented the higher affinity of them to Cu^{2+} ions, compared to larger particles. In DI water, the smaller $1/n$ value for PS-130 (Table 3), showed higher energetically

heterogeneous active sites, suggesting high-energy sites were prioritized during adsorption.[62] Conversely, larger particles had more homogeneously distributed active sites on the surface of PS-NPs.

Based on Fig. 8, higher adsorption was attained at lower temperatures, with smaller particles demonstrating greater susceptibility to temperature-induced changes. Consequently, increasing particle size resulted in a less noticeable variation in adsorption by temperature. The convex form of the isotherm graph for DI water exhibited a favourable adsorption profile, indicating a high degree of adsorption at low concentrations of Cu^{2+}.[63] In contrast, for seawater, the isotherm takes on a concave shape, suggesting unfavorable adsorption behavior at low concentrations and an improvement of adsorption at higher concentrations of metal ions. This type of isotherm (type III isotherm) is marked by weak adsorbate–adsorbent interactions, where adsorbate–adsorbate interactions dominate, leading to lower binding energy.[64] In this context, the adsorbate (Cu^{2+} ions and the salt ions of seawater) do not form strong bonds with the adsorbent (PS-NPs), resulting in weak adsorption. Additionally, the ions interactions with each other are stronger than their interactions with PS-NPa, resulting in clustering of adsorbates (Cu^{2+} ions and salt ions) on the surface of PS-NPs.[65] As the concentration increases further, it is expected that the adsorbent surface would become increasingly occupied, and the adsorption rate would start to level off as the adsorbent approaches saturation.[66]

For both media, the extent of the curvature diminishes with an increase in particle size, resulting in a more linear trend, approaching $1/n$ closer to 1 in Freundlich adsorption. Considering the role of $1/n$ in the shape of the isotherm fitting and consistent isotherm shape for a sample in a given medium, $1/n$ remained almost constant, while K_f changed across different temperatures. At each temperature increase to 300 K and 310 K, K_f decreased to 0.7 ± 0.1 of its value at the preceding lower temperature. On the other hand, by increasing the concentration of Cu^{2+} ions (higher than 20–30 mg L^{-1}), the changes in adsorption is more noticeable along with temperature while at lower concentration (up to 20 mg L^{-1}), the changes in adsorption is less dependant to temperature (Fig. 8). This can be attributed to the cumulative influence of temperature-related factors, such as the kinetic energy of the of adsorption.

4 Conclusion

In this study, PS-NPs were synthesized through surfactant-free emulsion polymerization with controlled particle size distribution, providing a size-dependent platform to study Cu^{2+} adsorption behaviour of polystyrene nanoparticles (PS-NPs). UV ageing induced morphological changes, including aggregation and colloidal instability due to photodegradation of sulfate groups, particularly pronounced in PS-130 nm particles. XPS analysis indicated oxidative modifications post UV-ageing, by creating carbonyl bonds, influencing Cu^{2+} adsorption binding states. Investigations into adsorption kinetics, described by
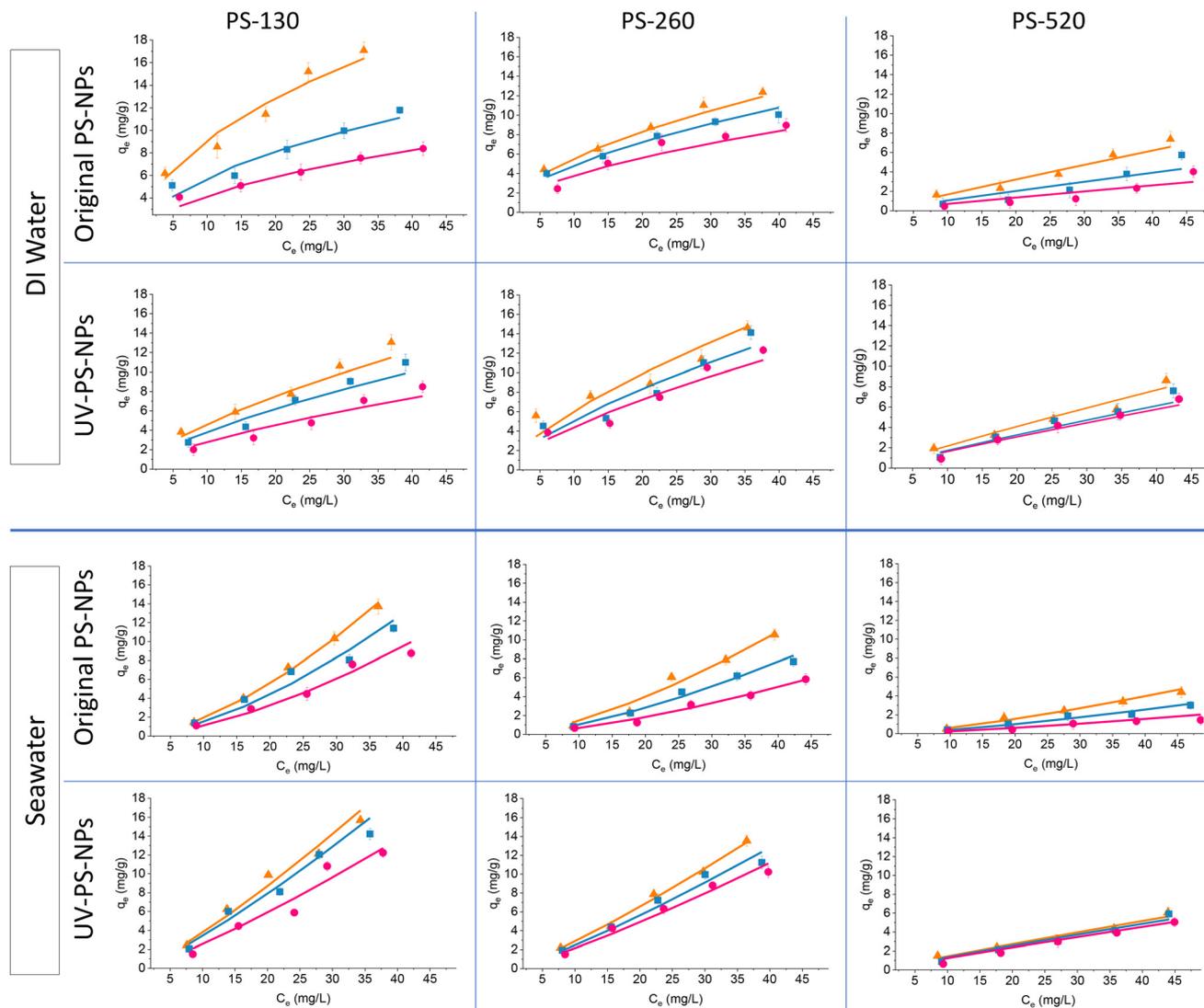
Fig. 8 The effect of temperature on the Cu^{2+} adsorption isotherms by different size ranges of original and UV-aged PS-NPs in DI water and seawater (290 K ▲, 300 K ■, 310 K ●).

Table 3 Coefficients of isotherm models fitted for adsorption of Cu^{2+} ions by original and UV-aged PS-NPs in DI water and seawater

	Medium	Particle size (nm)	Langmuir model			Freundlich model		
			K_l (L g^{-1})	q_m (mg g^{-1})	R_l^2	K_f (L g^{-1})	$1/n$	R_f^2
Original PS	DI water	130	0.139	17.24	0.881	2.974	0.486	0.941
		260	0.079	13.70	0.834	1.492	0.573	0.915
		520	0.013	15.62	0.917	0.190	0.945	0.938
	Seawater	130	0.021	6.66	0.988	0.052	1.560	0.998
		260	0.022	3.70	0.986	0.036	1.454	0.997
		520	0.016	3.03	0.967	0.028	1.343	0.979
UV-aged PS	DI water	130	0.054	14.49	0.833	0.951	0.690	0.895
		260	0.164	12.66	0.718	1.211	0.701	0.816
		520	0.011	22.22	0.973	0.267	0.911	0.944
	Seawater	130	0.016	18.52	0.973	0.232	1.210	0.977
		260	0.009	29.41	0.997	0.184	1.192	0.994
		520	0.022	9.09	0.941	0.161	0.924	0.930

pseudo-second-order kinetics, demonstrated the influence of size, UV ageing, and medium properties. In DI water, smaller particles (PS-130) initially showed enhanced adsorption capacities (mg g^{-1}), but post-UV ageing, PS-260 surpassed PS-

This journal is © The Royal Society of Chemistry 2025

Environ. Sci.: Nano, 2025, **12**, 548–562 | **559**

130. The equilibrium time doubled from 2 to 4 hours as the particle diameter increased from 130 to 260 nm. However, PS-520 exhibited an equilibrium time similar to PS-260, despite showing 4 times and 6 times less adsorption compared to PS-260 and PS-130, respectively. In seawater, the adsorption capacity decreased for all samples by 3–4 times compared to DI water, due to the presence of competitive cations, while equilibrium time decrease to less than 2 hours.

The calculation of activation energy, based on adsorption kinetics, proved the physical essence of Cu^{2+} ions adsorption across all the samples, indicating electrostatic and coordination bonding. This value is higher for UV-aged particles, proved to be as a result of prominent $Cu(OH)_2$ bonding between PS and Cu^{2+} ions, based on XPS analysis. The adsorption isotherm analysis indicated a preference for the Freundlich model, which tended to exhibit a more linear behaviour with increasing particle size and/or temperature. Smaller $1/n$ for smaller particles indicated higher heterogeneity of active sites, affecting the adsorption based on surface area. Distinctive isotherm shapes in DI water and seawater emphasized varied adsorption behaviours across Cu^{2+} concentrations. Convex isotherm shape in DI water indicated favourable adsorption, while type of isotherm for seawater showed unfavourable adsorption at lower concentrations, as well as weak adsorption between Cu^{2+} and PS-NPs, also confirmed by lower activation energies.

This study has advanced our understanding of PS-NPs behaviour in aquatic settings, elucidating the intricate relationships among particle size, UV-induced modifications of PS-NPs, and the influence of salt ions and temperature on adsorption characteristics. Given the existing knowledge gap regarding the interaction of polymeric nanoparticles and metal ions below 1 μm, this work contributes to our understanding in this field and may have implications for other polymer types within the nano-size range to enrich our understanding of metal/polymeric nanoparticle interactions in aquatic environments.

Data availability

The data supporting this article have been included as part of the ESI.†

Conflicts of interest

There are no conflicts of interest to declare.

Acknowledgements

References

1 H. Luo, C. Liu, D. He, J. Xu, J. Sun and J. Li, *et al.* Environmental behaviors of microplastics in aquatic systems: A systematic review on degradation, adsorption, toxicity and biofilm under aging conditions, *J. Hazard. Mater.*, 2022, **423**, 126915.

2 V. Godoy, G. Blázquez, M. Calero, L. Quesada and M. Martín-Lara, The potential of microplastics as carriers of metals, *Environ. Pollut.*, 2019, **255**, 113363.

3 D. Brennecke, B. Duarte, F. Paiva, I. Caçador and J. Canning-Clode, Microplastics as vector for heavy metal contamination from the marine environment, *Estuarine, Coastal Shelf Sci.*, 2016, **178**, 189–195.

4 N. Naqash, S. Prakash, D. Kapoor and R. Singh, Interaction of freshwater microplastics with biota and heavy metals: a review, *Environ. Chem. Lett.*, 2020, **18**(6), 1813–1824.

5 A. A. Koelmans, E. Besseling and W. J. Shim, Nanoplastics in the aquatic environment, Critical review, *Marine anthropogenic litter*, 2015, pp. 325–340.

6 A. Ter Halle, L. Jeanneau, M. Martignac, E. Jardé, B. Pedrono and L. Brach, *et al.* Nanoplastic in the North Atlantic subtropical gyre, *Environ. Sci. Technol.*, 2017, **51**(23), 13689–13697.

7 M. Sighicelli, L. Pietrelli, F. Lecce, V. Iannilli, M. Falconieri and L. Coscia, *et al.* Microplastic pollution in the surface waters of Italian Subalpine Lakes, *Environ. Pollut.*, 2018, **236**, 645–651.

8 M. Lang, X. Yu, J. Liu, T. Xia, T. Wang and H. Jia, *et al.* Fenton aging significantly affects the heavy metal adsorption capacity of polystyrene microplastics, *Sci. Total Environ.*, 2020, **722**, 137762.

9 X. Guo, Y. Liu and J. Wang, Equilibrium, kinetics and molecular dynamic modeling of Sr2+ sorption onto microplastics, *J. Hazard. Mater.*, 2020, **400**, 123324.

10 J. Yang, L. Cang, Q. Sun, G. Dong, S. T. Ata-Ul-Karim and D. Zhou, Effects of soil environmental factors and UV aging on Cu 2+ adsorption on microplastics, *Environ. Sci. Pollut. Res.*, 2019, **26**, 23027–23036.

11 G. Zhu, K. Yue, X. Ni, C. Yuan and F. Wu, The types of microplastics, heavy metals, and adsorption environments control the microplastic adsorption capacity of heavy metals, *Environ. Sci. Pollut. Res.*, 2023, **30**(33), 80807–80816.

12 Y. Li, Y. Zhang, F. Su, Y. Wang, L. Peng and D. Liu, Adsorption behaviour of microplastics on the heavy metal Cr (VI) before and after ageing, *Chemosphere*, 2022, **302**, 134865.

13 K. Lu, R. Qiao, H. An and Y. Zhang, Influence of microplastics on the accumulation and chronic toxic effects of cadmium in zebrafish (Danio rerio), *Chemosphere*, 2018, **202**, 514–520.

14 R. M. Town, H. P. Van Leeuwen and R. Blust, Biochemodynamic features of metal ions bound by micro-and nano-plastics in aquatic media, *Front. Chem.*, 2018, **6**, 627.

15 J. Gigault, A. Ter Halle, M. Baudrimont, P. Y. Pascal, F. Gauffre and T. L. Phi, *et al.* Current opinion: what is a nanoplastic?, *Environ. Pollut.*, 2018, **235**, 1030–1034.

560 | *Environ. Sci.: Nano*, 2025, **12**, 548–562

This journal is © The Royal Society of Chemistry 2025

16 F. Yu, C. Yang, Z. Zhu, X. Bai and J. Ma, Adsorption behavior of organic pollutants and metals on micro/nanoplastics in the aquatic environment, *Sci. Total Environ.*, 2019, **694**, 133643.

17 A. Brewer, I. Dror and B. Berkowitz, The mobility of plastic nanoparticles in aqueous and soil environments: a critical review, *ACS ES&T Water*, 2020, **1**(1), 48–57.

18 E. Besseling, J. T. Quik, M. Sun and A. A. Koelmans, Fate of nano-and microplastic in freshwater systems: A modeling study, *Environ. Pollut.*, 2017, **220**, 540–548.

19 S. Maity, C. Biswas, S. Banerjee, R. Guchhait, M. Adhikari and A. Chatterjee, *et al.* Interaction of plastic particles with heavy metals and the resulting toxicological impacts: a review, *Environ. Sci. Pollut. Res.*, 2021, 1–17.

20 R. Qiao, K. Lu, Y. Deng, H. Ren and Y. Zhang, Combined effects of polystyrene microplastics and natural organic matter on the accumulation and toxicity of copper in zebrafish, *Sci. Total Environ.*, 2019, **682**, 128–137.

21 P. Liu, L. Qian, H. Wang, X. Zhan, K. Lu and C. Gu, *et al.* New insights into the aging behavior of microplastics accelerated by advanced oxidation processes, *Environ. Sci. Technol.*, 2019, **53**(7), 3579–3588.

22 R. Lehner, C. Weder, A. Petri-Fink and B. Rothen-Rutishauser, Emergence of nanoplastic in the environment and possible impact on human health, *Environ. Sci. Technol.*, 2019, **53**(4), 1748–1765.

23 R. Mao, M. Lang, X. Yu, R. Wu, X. Yang and X. Guo, Aging mechanism of microplastics with UV irradiation and its effects on the adsorption of heavy metals, *J. Hazard. Mater.*, 2020, **393**, 122515.

24 T. Toapanta, E. D. Okoffo, S. Ede, S. O'Brien, S. D. Burrows and F. Ribeiro, *et al.* Influence of surface oxidation on the quantification of polypropylene microplastics by pyrolysis gas chromatography mass spectrometry, *Sci. Total Environ.*, 2021, **796**, 148835.

25 K. Zhu, H. Jia, Y. Sun, Y. Dai, C. Zhang and X. Guo, *et al.* Long-term phototransformation of microplastics under simulated sunlight irradiation in aquatic environments: roles of reactive oxygen species, *Water Res.*, 2020, **173**, 115564.

26 K. Zhang, A. H. Hamidian, A. Tubić, Y. Zhang, J. K. Fang and C. Wu, *et al.* Understanding plastic degradation and microplastic formation in the environment: A review, *Environ. Pollut.*, 2021, 116554.

27 Q. Wang, Y. Zhang, X. Wangjin, Y. Wang, G. Meng and Y. Chen, The adsorption behavior of metals in aqueous solution by microplastics effected by UV radiation, *J. Environ. Sci.*, 2020, **87**, 272–280.

28 C. Chen, F. Wei, L. Ye, Y. Wang, L. Long and C. Xu, *et al.* Adsorption of Cu^{2+} by UV aged polystyrene in aqueous solution, *Ecotoxicol. Environ. Saf.*, 2022, **232**, 113292.

29 J. Ma, J. Zhao, Z. Zhu, L. Li and F. Yu, Effect of microplastic size on the adsorption behavior and mechanism of triclosan on polyvinyl chloride, *Environ. Pollut.*, 2019, **254**, 113104.

30 D. Kim, Y. Chae and Y. J. An, Mixture toxicity of nickel and microplastics with different functional groups on Daphnia magna, *Environ. Sci. Technol.*, 2017, **51**(21), 12852–12858.

31 X. Gao, I. Hassan, Y. Peng, S. Huo and L. Ling, Behaviors and influencing factors of the heavy metals adsorption onto microplastics: A review, *J. Cleaner Prod.*, 2021, **319**, 128777.

32 Y. Dong, M. Gao, Z. Song and W. Qiu, As (III) adsorption onto different-sized polystyrene microplastic particles and its mechanism, *Chemosphere*, 2020, **239**, 124792.

33 H. El Hadri, J. Gigault, B. Maxit, B. Grassl and S. Reynaud, Nanoplastic from mechanically degraded primary and secondary microplastics for environmental assessments, *NanoImpact*, 2020, **17**, 100206.

34 J. Caldwell, R. Lehner, S. Balog, C. Rhême, X. Gao and D. Septiadi, *et al.* Fluorescent plastic nanoparticles to track their interaction and fate in physiological environments, *Environ. Sci.: Nano*, 2021, **8**(2), 502–513.

35 J. Seghers, E. A. Stefaniak, R. La Spina, C. Cella, D. Mehn and D. Gilliland, *et al.* Preparation of a reference material for microplastics in water–evaluation of homogeneity, *Anal. Bioanal. Chem.*, 2022, **414**, 385–397.

36 A. G. Rodríguez-Hernández, J. A. Muñoz-Tabares, J. C. Aguilar-Guzmán and R. Vazquez-Duhalt, A novel and simple method for polyethylene terephthalate (PET) nanoparticle production, *Environ. Sci.: Nano*, 2019, **6**(7), 2031–2036.

37 K. Tanaka, Y. Takahashi, H. Kuramochi, M. Osako, S. Tanaka and G. Suzuki, Preparation of nanoscale particles of five major polymers as potential standards for the study of nanoplastics, *Small*, 2021, **17**(49), 2105781.

38 G. Balakrishnan, M. Déniel, T. Nicolai, C. Chassenieux and F. Lagarde, Towards more realistic reference microplastics and nanoplastics: preparation of polyethylene micro/nanoparticles with a biosurfactant, *Environ. Sci.: Nano*, 2019, **6**(1), 315–324.

39 S. Comber, G. Deviller, I. Wilson, A. Peters, G. Merrington and P. Borrelli, *et al.* Sources of copper into the European aquatic environment, *Integr. Environ. Assess. Manage.*, 2023, **19**(4), 1031–1047.

40 S. E. Shim, K. Kim, S. Oh and S. Choe, Preparation of ultra fine poly (methyl methacrylate) microspheres in methanol-enriched aqueous medium, *Macromol. Res.*, 2004, **12**, 240–245.

41 J. E. Arikibe and S. Prasad, Determination and comparison of selected heavy metal concentrations in seawater and sediment samples in the coastal area of Suva, Fiji, *Mar. Pollut. Bull.*, 2020, **157**, 111157.

42 J. P. Simonin, On the comparison of pseudo-first order and pseudo-second order rate laws in the modeling of adsorption kinetics, *Chem. Eng. J.*, 2016, **300**, 254–263.

43 V. Kinigopoulou, I. Pashalidis, D. Kalderis and I. Anastopoulos, Microplastics as carriers of inorganic and organic contaminants in the environment: A review of recent progress, *J. Mol. Liq.*, 2022, 118580.

44 I. Langmuir, The adsorption of gases on plane surfaces of glass, mica and platinum, *J. Am. Chem. Soc.*, 1918, **40**(9), 1361–1403.

45 A. Taha, M. A. Shreadah, A. Ahmed and H. F. Heiba, Multi-component adsorption of Pb (II), Cd (II), and Ni (II) onto Egyptian Na-activated bentonite; equilibrium, kinetics, thermodynamics, and application for seawater desalination, *J. Environ. Chem. Eng.*, 2016, **4**(1), 1166–1180.

This journal is © The Royal Society of Chemistry 2025

Environ. Sci.: Nano, 2025, **12**, 548–562 | 561

46 A. W. Marczewski, Analysis of kinetic Langmuir model. Part I: integrated kinetic Langmuir equation (IKL): a new complete analytical solution of the Langmuir rate equation, *Langmuir*, 2010, **26**(19), 15229–15238.

47 H. Freundlich, Über die adsorption in lösungen, *Z. Phys. Chem.*, 1907, **57**(1), 385–470.

48 J. Li and H. Zhang, Adsorption-desorption of oxytetracycline on marine sediments: kinetics and influencing factors, *Chemosphere*, 2016, **164**, 156–163.

49 P. A. Lovell and F. J. Schork, Fundamentals of emulsion polymerization, *Biomacromolecules*, 2020, **21**(11), 4396–4441.

50 X. Wang, Y. Li, J. Zhao, X. Xia, X. Shi and J. Duan, *et al.* UV-induced aggregation of polystyrene nanoplastics: effects of radicals, surface functional groups and electrolyte, *Environ. Sci.: Nano*, 2020, **7**(12), 3914–3926.

51 C. V. Cushman, S. Chatterjee, G. H. Major, N. J. Smith, A. Roberts and M. R. Linford, Trends in Advanced XPS Instrumentation, *Vac. Technol. Coat.*, 2017, **9**, 25–31.

52 K. O. Adebowale, I. E. Unuabonah and B. I. Olu-Owolabi, The effect of some operating variables on the adsorption of lead and cadmium ions on kaolinite clay, *J. Hazard. Mater.*, 2006, **134**(1–3), 130–139.

53 F. Zhang, Z. Wang, S. Wang, H. Fang and D. Wang, Aquatic behavior and toxicity of polystyrene nanoplastic particles with different functional groups: complex roles of pH, dissolved organic carbon and divalent cations, *Chemosphere*, 2019, **228**, 195–203.

54 N. Singh, E. Tiwari, N. Khandelwal and G. K. Darbha, Understanding the stability of nanoplastics in aqueous environments: effect of ionic strength, temperature, dissolved organic matter, clay, and heavy metals, *Environ. Sci.: Nano*, 2019, **6**(10), 2968–2976.

55 A. Wegner, E. Besseling, E. M. Foekema, P. Kamermans and A. A. Koelmans, Effects of nanopolystyrene on the feeding behavior of the blue mussel (Mytilus edulis L.), *Environ. Toxicol. Chem.*, 2012, **31**(11), 2490–2497.

56 O. S. Alimi, J. Farner Budarz, L. M. Hernandez and N. Tufenkji, Microplastics and nanoplastics in aquatic environments: aggregation, deposition, and enhanced contaminant transport, *Environ. Sci. Technol.*, 2018, **52**(4), 1704–1724.

57 E. Cano, C. Torres and J. Bastidas, An XPS study of copper corrosion originated by formic acid vapour at 40% and 80% relative humidity, *Mater. Corros.*, 2001, **52**(9), 667–676.

58 H. Azimi, S. Kuhri, A. Osvet, G. Matt, L. S. Khanzada and M. Lemmer, *et al.* Effective ligand passivation of Cu2O nanoparticles through solid-state treatment with mercaptopropionic acid, *J. Am. Chem. Soc.*, 2014, **136**(20), 7233–7236.

59 P. Liu, K. Lu, J. Li, X. Wu, L. Qian and M. Wang, *et al.* Effect of aging on adsorption behavior of polystyrene microplastics for pharmaceuticals: Adsorption mechanism and role of aging intermediates, *J. Hazard. Mater.*, 2020, **384**, 121193.

60 M. E. Argun, Use of clinoptilolite for the removal of nickel ions from water: kinetics and thermodynamics, *J. Hazard. Mater.*, 2008, **150**(3), 587–595.

61 Y. Wang, X. Wang, Y. Li, J. Li, F. Wang and S. Xia, *et al.* Biofilm alters tetracycline and copper adsorption behaviors onto polyethylene microplastics, *Chem. Eng. J.*, 2020, **392**, 123808.

62 X. Guo, J. Pang, S. Chen and H. Jia, Sorption properties of tylosin on four different microplastics, *Chemosphere*, 2018, **209**, 240–245.

63 A. Gabelman, Adsorption basics: part 1, *Chem. Eng. Prog.*, 2017, **113**(7), 48–53.

64 K. V. Kumar, S. Gadipelli, B. Wood, K. A. Ramisetty, A. A. Stewart and C. A. Howard, *et al.* Characterization of the adsorption site energies and heterogeneous surfaces of porous materials, *J. Mater. Chem. A*, 2019, **7**(17), 10104–10137.

65 M. Alaqarbeh, Adsorption phenomena: definition, mechanisms, and adsorption types: short review, *Rhazes: Green Appl. Chem.*, 2021, **13**, 43–51.

66 M. Burhan, M. W. Shahzad and K. C. Ng, Energy distribution function based universal adsorption isotherm model for all types of isotherm, *Int. J. Low-Carbon Technol.*, 2018, **13**(3), 292–297.

562 | *Environ. Sci.: Nano*, 2025, **12**, 548–562

This journal is © The Royal Society of Chemistry 2025